

Chapter 4

High Transition Temperature Superconducting Composite Microbolometers

4.1 Superconducting Materials for Bolometric Detection

Superconducting materials exhibit unique properties which make them especially applicable for thermal detectors. Just above the critical temperature (T_c) of a superconductor (defined as the highest temperature at which the material will carry superconducting current), the material exhibits a sharp change in resistivity. If the temperature of the material is raised above this temperature, the material will change from a superconducting state to a normal state. The temperatures below the onset of superconductivity and above T_c correspond to the transition region. Within the transition region, the steep change in resistivity ($\alpha \sim 1 \text{ K}^{-1}$) will be much higher than for normal materials, such as bismuth ($\alpha \sim 0.003 \text{ K}^{-1}$). Figure 4.1 shows a plot of the resistance versus temperature for a strip of superconducting material.

Until recently, all known superconducting materials had very low critical temperatures ($T_c < 20 \text{ K}$), and most apparatuses which used these materials required cooling with liquid helium. The discovery of a new class of superconducting materials has extended the critical temperature to above 77K, so that liquid nitrogen can be used to cool these materials. In addition to being much cheaper than liquid helium, liquid nitrogen is also much easier to store and use. The first high transition temperature (HiTc) superconductor found to have a transition temperature above liquid nitrogen was Y-Ba-Cu-O, with $T_c \sim 90\text{K}$. Another system, made up of Bi-Sr-Ca-Cu-O, was found to have two separate superconducting phases of different stoichiometries, with transition temperatures near 85K and 110K. Another material system made of Tl-Ca-Ba-Cu-O was discovered which has a $T_c \sim 125\text{K}$. The high thermal sensitivity of superconductors has provided much motivation for adapting these materials as thermal detector elements. Large area conventional bolometers have already been studied and tested using HiTc materials [1-5].

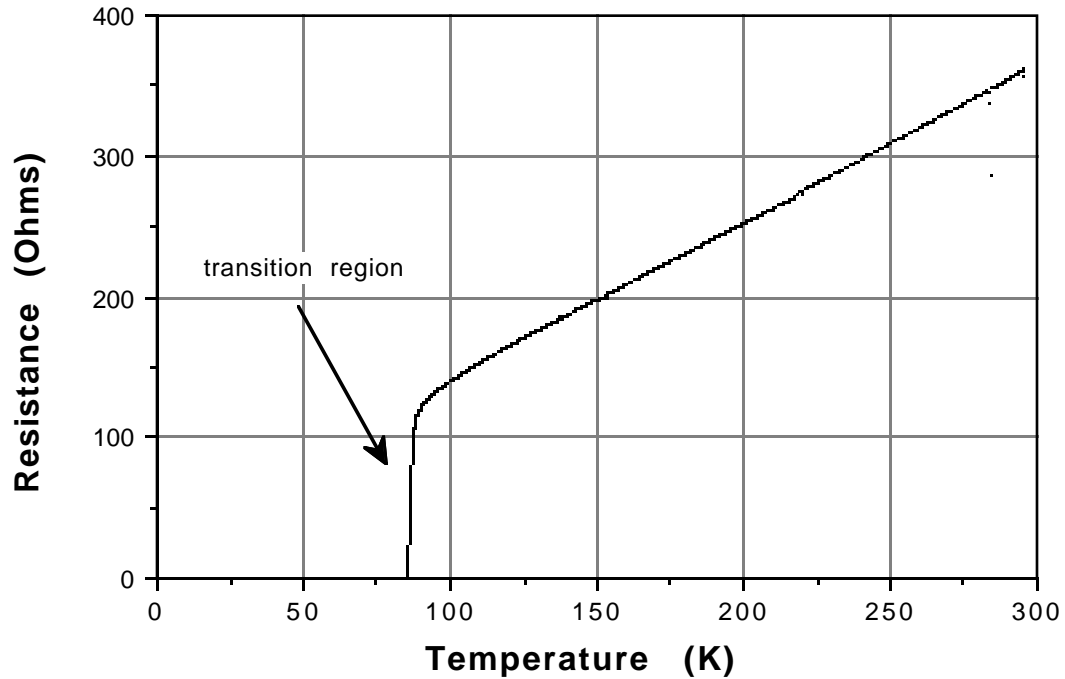


Figure 4.1 Resistance versus temperature for a strip of Y-Ba-Cu-Oxide.

4.2 Superconducting Antenna-Coupled Microbolometers

The idea of coupling a superconducting microbolometer to a planar antenna structure was first suggested by Neikirk [6]. Careful attention must be given to the device material choices in order to optimize the performance of the system. Since radiation more readily enters the antenna through the back of the substrate, the substrate material must be reasonably transparent to the desired spectral range. The dielectric constant of the substrate should be low in order to provide a better feed pattern for the optics, and will usually give a better overall system coupling efficiency. The thermal conductivity of the substrate should be low, or else there should be a thermal barrier between the microbolometer and the substrate. There have been reports of thermal boundaries [7-9] between the HiTc materials and the underlying substrates. A thermal

boundary would enhance the thermal sensitivity of HiTc based detectors by reducing the rate of heat loss into the substrate.

Most conventional superconducting materials (such as Pb, Sn, and Nb) can be fully fabricated by purely physical deposition techniques, such as evaporation or sputtering. Virtually any substrate material can be used for these materials. The HiTc materials, in addition to being deposited, require annealing ($\sim 700 - 900$ °C) in an oxygen environment, either during film growth, or after deposition. Interdiffusion between the substrate and the HiTc films during annealing is also a problem with many substrate materials. Very few substrate materials are available which are compatible with these harsh growth conditions. Table 4.1 compares some of the relevant properties of some substrates used for far-infrared-millimeter wave applications and/or HiTc materials.

Material	Thermal conductivity k (W/cm/°C)	Dielectric constant ϵ
Quartz (fused silica)	0.014 ²	4.3 ¹
Sapphire	0.46 (@ 300 K) 9.6 (@ 80 K)	8.6 \pm 4 10.55 // ⁴
MgO	4.5 ⁴ (@ 80 K)	9.7 ⁴
Si	1.48 (@300 K) 13.4 (@80K)	11.8
LaAlO ₃	-	15 ⁵
YSZ	0.0105 ⁴ (@ 260K)	12.0 ⁴

Table 4.1 Properties of Various Substrate Materials

1. CRC Handbook of Chemistry and Physics, 64th edition, CRC Press, Boca Raton, FL, 1984.
2. Materials Handbook for Hybrid Microelectronics, Artech House; Boston, MA, 1988.
3. Thermophysical Properties of Matter (Volume 2); Thermal Conductivity, Non Metallic Solids, IFI/Plenum, 1970.
4. Handbook of Infrared Optical Materials, edited by Paul Klocek; Marcel Dekker, Inc., New York, 1991.
5. Alan, B. Berezin, "A Low Noise High Temperature Superconducting Quantum Interference Device," Ph.D. Dissertation, University of Texas at Austin, 1993

Impedance matching with an antenna structure is another issue when considering superconducting materials as detector elements. The low resistivity of HiTc superconductors ($r \sim 20$ to 60 mW-cm) near the middle of the transition makes it difficult to match the detector impedance to typical antenna structures. One solution to this problem is to lengthen the detector so that its resistance matches the antenna impedance. However, the long lengths required would significantly lower the thermal

impedance of the microbolometer as well as increase the thermal mass, thus lowering its sensitivity, and likely its speed of operation. Another problem with long detectors is that for short wavelengths ($\lambda \sim < 2 \times$ detector length), the detector behaves more like a lossy microstrip [10], rather than a lumped element. Although an antenna-coupled microstrip detector may actually work to some extent, the load element impedance will have a frequency dependent impedance, and its integration with a planar antenna would be difficult to model. One group has reported [11] matching a Nb load element by making the film extremely thin (200 Å). It should be noted that it would be very difficult to fabricate a high quality HiTc film of this thickness.

There have been reports [10-12] of antenna-coupled microbolometers which used high dielectric constant substrates that provided a somewhat lower impedance for the antenna structure. These studies used complimentary antenna designs, in which the metal covered regions are the same shape as the bare substrate. Strictly speaking, these antennas were not self-complimentary, since the dielectric was not identical on both sides of the antenna. However, this assumption was made in order to approximate the antenna impedance. A true self-complementary antenna design will have a real antenna impedance of

$$\text{Re(Im pedance)} = \frac{377}{\sqrt{2(1 + \epsilon)}} \quad (4.1)$$

that only depends on the dielectric constant (ϵ) of the substrate, and is independent of frequency. By using a substrate with a high dielectric constant, a somewhat lower antenna impedance can be obtained. Using this approximation, a YSZ substrate ($\epsilon \sim 12$) will yield an antenna impedance of $\sim 75 \Omega$, compared to 120Ω for a 90° bow tie antenna on quartz ($\epsilon \sim 4$). Given a minimum line width of $2 \mu\text{m}$, a 750 \AA thick film of YBCO (of resistivity = $60 \text{ m}\Omega\text{-cm}$) would need to be $\sim 19 \mu\text{m}$ long in order to match with an antenna with an embedding impedance of 75Ω . While high dielectric constant substrates may help to adapt low resistivity materials to antenna structures, this may cause problems with the overall coupling efficiency of the system.

It was suggested by Wentworth[13] that a twin slot antenna could possibly be used to match the low impedances of superconducting materials, since it is theoretically possible to achieve antenna impedances as low as 5Ω with this antenna design.

Typically, twin slot antennas have been built by using a polyimide layer to support the detector above a metal ground plane [14]. Currently, however, high T_c superconducting films cannot be fabricated on polyimide. However, this problem may possibly be overcome by building the detector on the substrate, and using the polyimide to support the ground plane over the detector.

Another solution would be to use the composite microbolometer structure (described in chapter 1) which separates the temperature sensing element from the antenna load element. This design has already been demonstrated with a tellurium element in conjunction with a nichrome heater element. [15]. Figure 4.2 shows a similar design where an impedance matched heater element is in close thermal contact with a YBCO detector element.

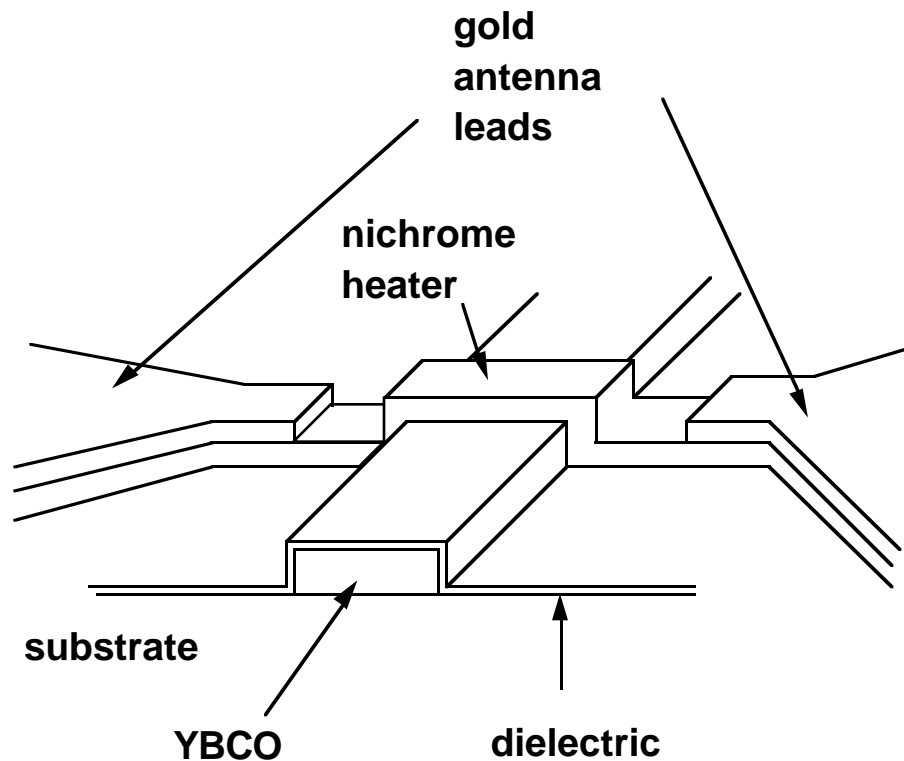


Figure 4.2 Composite Microbolometer design which uses a nichrome heater in close thermal contact with a YBCO detector. A thin dielectric layer isolates the heater from the detector.

4.3 Substrate Choice

Of the materials listed in table 4.1, only sapphire, MgO, YSZ, and LaAlO₃ can be used as substrates on which YBCO can be readily grown. Quartz is often used for microwave applications, though it is difficult to grow quality HiTc films on this material. High quality YBCO films can be grown directly on MgO, YSZ, LaAlO₃ and can be grown on sapphire with a buffer layer. Silicon is fairly transparent in the 1 to 10 μm range, but presents film growth problems as a HiTc substrate. By using a composite structure, antenna impedance issues do not affect the choices for the detector or substrate materials.

Of the materials that are left, there seems to be a trade-off between materials of low thermal conductivity and high dielectric constant, and materials of high thermal conductivity and low dielectric constant. For example, YSZ is a compatible substrate material with a low thermal conductivity; however, it has a relatively high dielectric constant. Sapphire has a lower dielectric constant, although the thermal conductivity is much higher. It would be useful to be able to predict the effects of these parameters in order to help optimize the performance of the microbolometer.

In order to model the effects of substrate thermal conductivity on the performance, a three dimensional finite difference technique was used to examine this parameter. An actual device was also fabricated and compared with these results. The working device also demonstrated that such a design would work using HiTc materials.

4.4 Thermal Simulations

For this set of experiments, a composite microbolometer was designed which used YBCO as the detector material. The dimensions used in the thermal model were the same as those of the device that was fabricated. Figure 4.3a shows an overhead view of the detector region. Device symmetry allowed the region being modeled to be reduced to the region enclosed by the dashed line. Figure 4.2b shows a tilted view of the region modeled. In order to input this information into the thermal model, the device had to be represented as a group of rectangularly shaped blocks, or elements. Figures 4.5a and 4.5b show the layout and numbering scheme used for this purpose.

The film used as the heater material (nichrome) is represented as elements 5, 6, 7, and 8. The power dissipated in the heater by joule heating was modeled as being distributed uniformly over elements 5, 6 and 7. Since element 8 was covered by a low resistance gold lead (element 9), joule heating in the region represented by this element was ignored.

Current fabrication techniques require that some substrates have a thin buffer layer of inert material between the substrate and the HiTc material. Sapphire substrates, for instance, can be used to support high quality YBCO films by using a thin (400 Å) layer of MgO between the sapphire and the YBCO film [16]. The numerical simulations here do not account for a buffer layer. However, since MgO and sapphire have similar thermal conductivities, this approximation should be accurate for this case. There have been reports of thermal boundaries that exist between HiTc films and the substrates [7-9]. The existence of a thermal boundary would be expected to increase the dc thermal impedance a detector. Thermal boundaries were not included in these models.

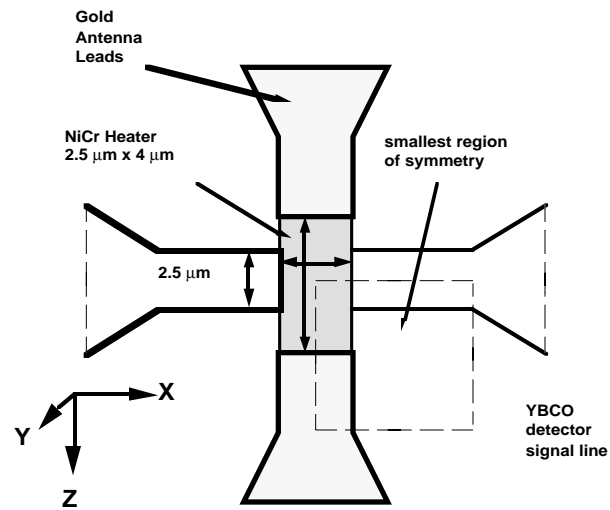


Figure 4.3 Overhead view of a composite microbolometer. Device symmetry allowed the region being modeled to be reduced to the region enclosed by the dashed line.

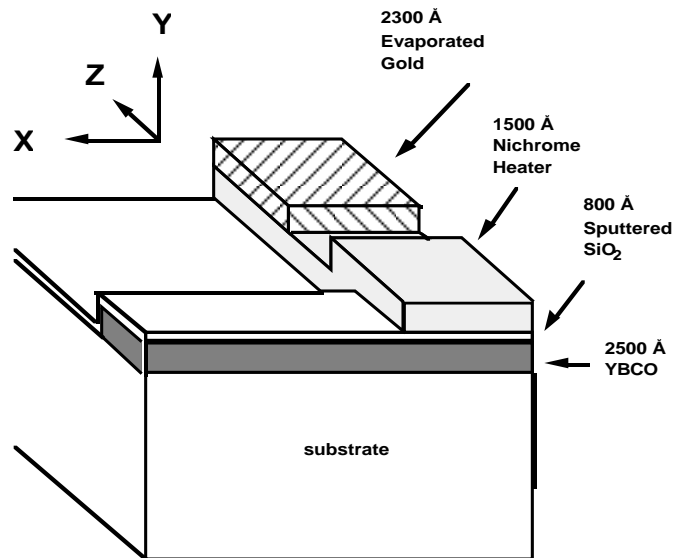
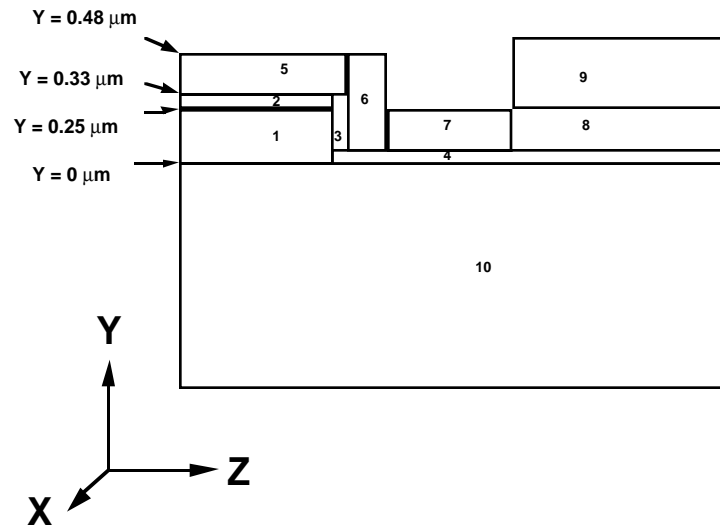
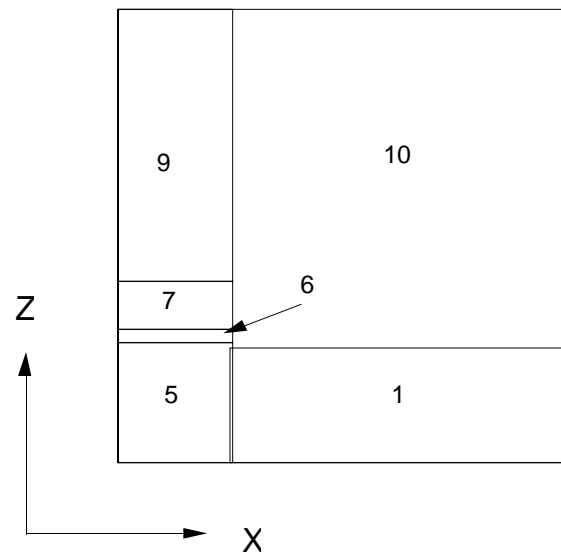


Figure 4.4 A tilted view of the region being modeled.



a) Side view



b) Overhead view

Figure 4.5 Layout and number scheme used to represent the composite microbolometer in a three dimensional finite difference model.

Some insight into the dominant heat loss modes can be gained by looking at the thermal profiles calculated by the thermal model. In particular, figure 4.6 gives some quantitative as well as qualitative information about the cooling mechanisms of the YBCO detector element. This figure shows the temperature profile in the **Y**-direction measured from the center of the detector. The most obvious conclusion is that substrates of low thermal conductivity result in higher detector temperatures. This figure also shows that for highly conductive substrates ($k_{\text{sub}} > \sim 1 \text{ W/cm/K}$), the average detector temperature in the center of the substrate is controlled by conductance through the detector, and is mostly independent of the substrate thermal conductivity.

The slope of the temperature profiles in figure 4.6 is an indication of the heat flux in the **Y**-direction (into the substrate). Note that the heat flux into the substrate (slope inside the YBCO) is nearly the same for all values of k_{sub} . This indicates that not much heat flux is diverted into the leads as the thermal conductivity of the substrate is changed over these values.

Figure 4.7 shows the effective composite thermal impedance for various substrate thermal conductivities. The effective impedance shown here describes a characteristic temperature rise in the detector due to power dissipated in the heater. For this value, an active region of the detector is defined as the region that lies directly below the heater region. For this example, the active region would be a $2.5 \mu\text{m} \times 2.5 \mu\text{m} \times 0.25 \mu\text{m}$ region of YBCO. The characteristic temperature rise was measured at $\mathbf{X} = 0.625 \mu\text{m}$, $\mathbf{Y} = 0.125 \mu\text{m}$, and $\mathbf{Z} = 0.625 \mu\text{m}$ (see figures 4.3 and 4.4). This point was chosen to approximate the average temperature rise of the active region, and lies halfway between the center and boundaries of the active region in the **X** and **Z** directions, and lies in the center of the film in the **Y**-direction.

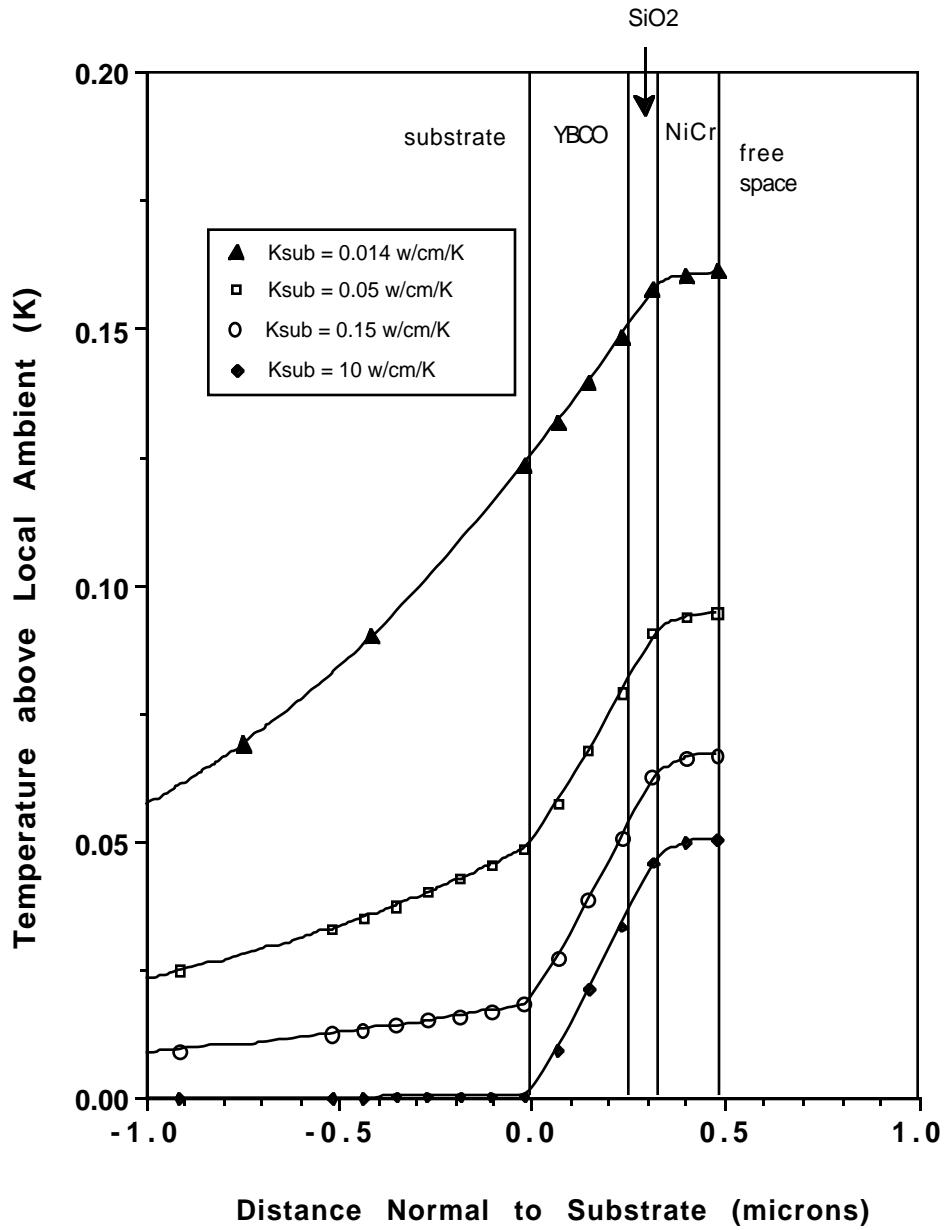


Figure 4.6

Thermal profiles into the substrate for composite microbolometers made of substrates of different thermal conductivities. The results are numerical simulations based on the layout described in figures 4.2 - 4.4, using an input power of 4 microwatts into the NiCr heater element.

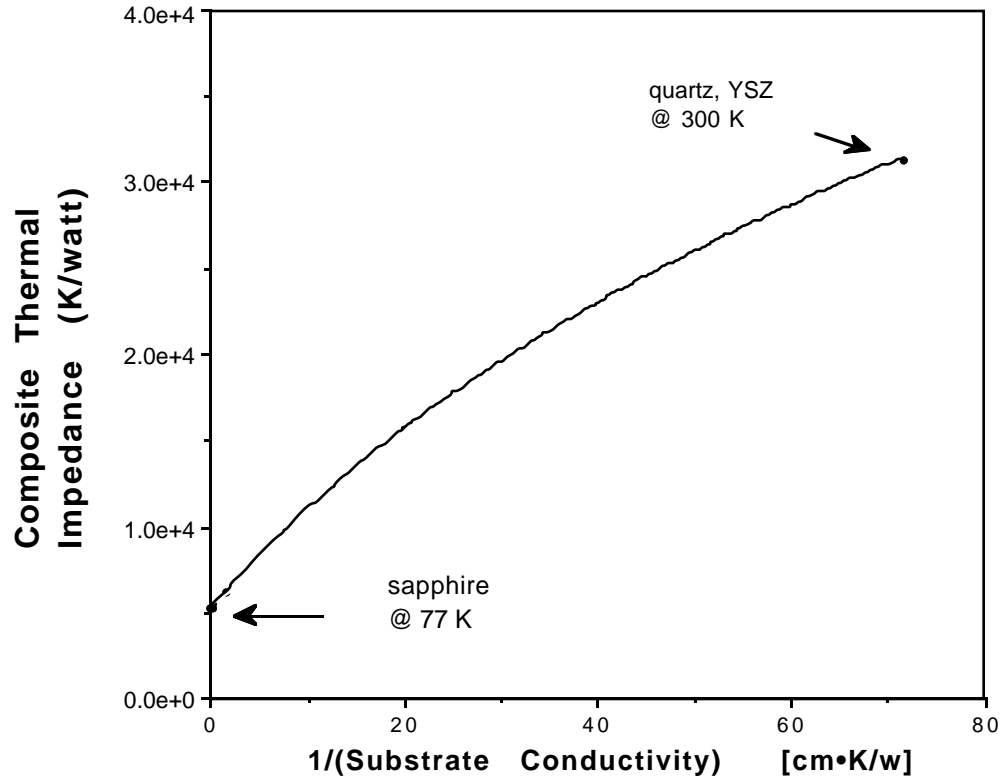


Figure 4.7 Effective composite thermal impedance for various substrate thermal conductivities

The fact that the effective thermal impedance intercepts the Y-axis for high values of k_{sub} , suggests that the device temperature would be insensitive to k_{sub} for high values of k_{sub} ($k_{\text{sub}} > \sim 1 \text{ W/cm/K}$). For low k_{sub} , the effective impedance remains strongly dependent on k_{sub} . For very low values, we would eventually expect heat flow to be limited by conductance through the leads. A slight flattening of the curve is seen in figure 4.7 as $1/k_{\text{sub}}$ increases, suggesting that only a small amount of heat flow is being diverted into the leads over the range of expected values of k_{sub} for the device geometry shown.

Figure 4.8 shows the device responsivity versus k_{sub} , based on using a sapphire substrate at 85K. These responsivities were calculated using the effective impedance values shown in figure 4.7. These values assume a 1 mA bias current, a device resistivity ρ of 60 mW-cm, and a thermal coefficient of resistivity of the detector $\alpha = 1$. The data here suggests only a modest improvement in responsivity over bismuth microbolometers ($r \sim 20$ V/W) of the same size. The existence of a thermal boundary between the HiTc film and the substrate may improve performance for an actual device. These steady state thermal simulations predict that the responsivity would increase by a factor of seven by varying the thermal conductivity of the substrate from 1 w/cm/K to 0.14 W/cm/K. For substrate thermal conductivities above ~ 0.5 W/cm/K, the dc responsivity was nearly independent of substrate thermal conductivity.

Using a substrate with a high thermal conductivity, such as sapphire, would be expected to increase the speed of the device while lowering the responsivity. Figure 4.9 shows the microbolometer temperature response at the end of a step pulse of power, as a function of pulse time. The results shown here were calculated using the transient finite difference method discussed in chapter 3. This figure shows a 3 dB drop in thermal response at $\sim 10^{-7}$ seconds, corresponding to ~ 10 MHz, which would be faster than the 3 dB cut-off frequency of 400 kHz that was reported for an $3.5 \mu\text{m} \times 4 \mu\text{m}$ bismuth air-bridge bolometer [17]. Responsivity data reported for conventional glass supported bismuth microbolometer [17] and a composite microbolometer using a tellurium detector element [15] shows 3 dB cut-off frequencies near 200 kHz and 20 kHz, respectively. This data suggests that although the dc responsivity for a high T_c device on sapphire may not be extraordinary, the devices would be able to operate at much faster speeds.

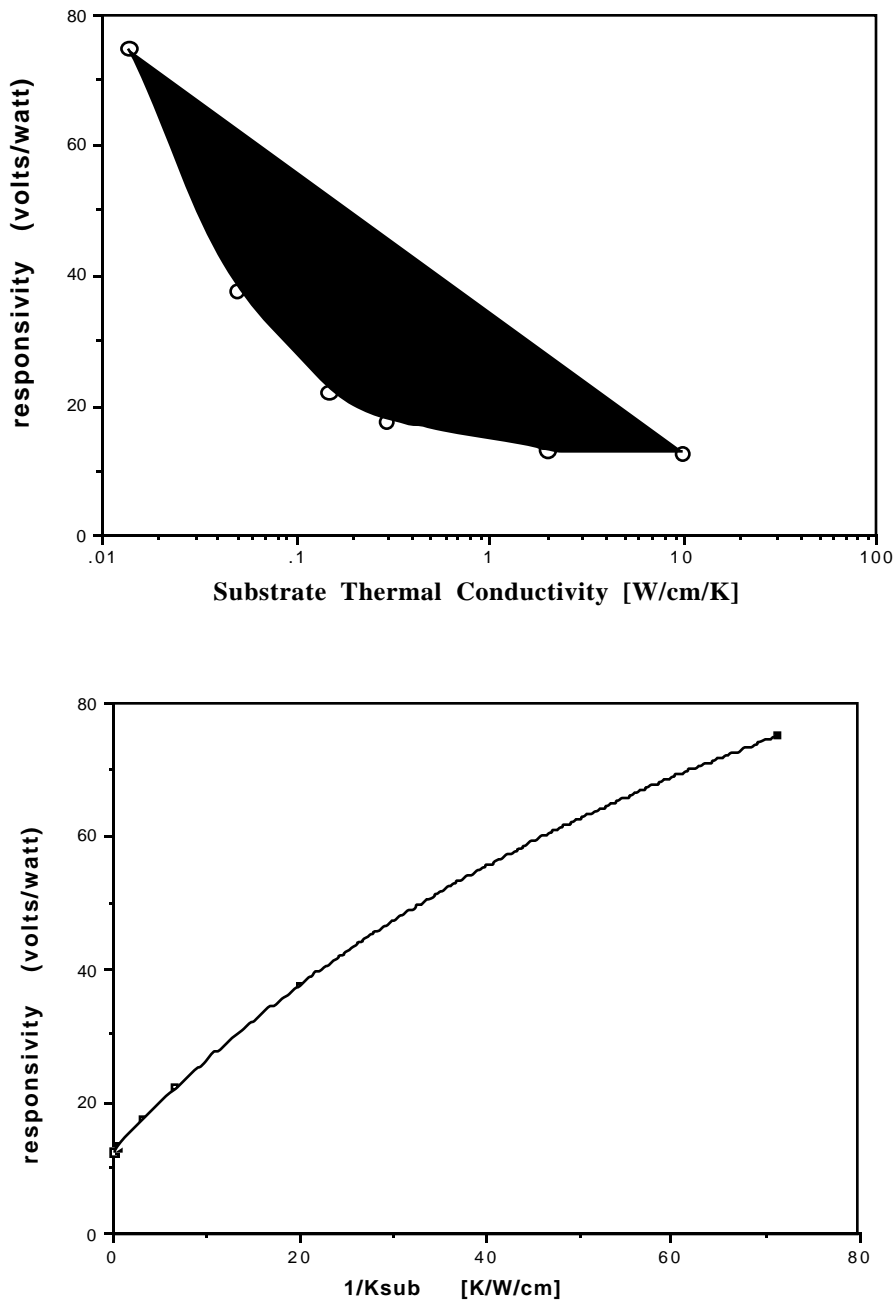


Figure 4.8 Device responsivity versus substrate thermal conductivity based on the effective impedance values shown in figure 4.6. These values assume a 1 mA bias current, a device resistivity of $60 \mu\Omega\text{-cm}$, and a device $\alpha = 1.0$. Both graphs represent the same set of data.

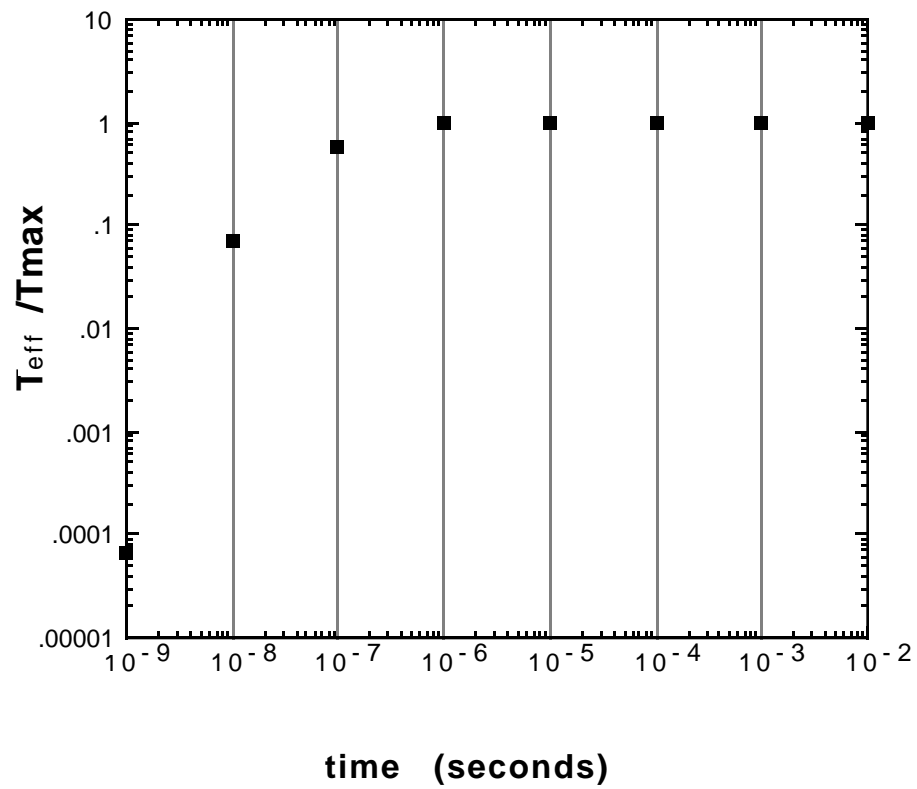


Figure 4.9 Composite microbolometer response to a step pulse of power as a function of pulse length.

4.5 Device Fabrication

The microbolometers that were fabricated for this experiment were built in a composite structure using the layout and dimensions shown in figures 4.3 and 4.4. The devices utilized a YBCO detector line on a buffered sapphire substrate. A 400 Å layer of MgO was used as the buffer between the YBCO and the sapphire. The YBCO films were prepared by co-evaporation of Y, Ba, and Cu in a low pressure oxygen environment [16]. These films were prepared and donated by Professor Alex de Lozanne's research group from the Department of Physics at the University of Texas at Austin.

The first step in fabrication involves patterning the YBCO film to form the detector line. An overview of this process will be given here, while the details are listed in appendix D. Ethylene-diamine-tetra-acetate (EDTA), which is often used as a food preservative, was used as the etchant to remove YBCO from the substrate. A pasty scum was left on the surfaces where the YBCO was removed. I found it important to remove as much of this scum as possible in order to have good adhesion for subsequent film materials. Although most of this scum could be removed by scrubbing with a wet Q-tip, the underlying material still did not provide a good adhesive surface for metalization. To deal with this problem, I modified the first mask so that the metal bonding pads were completely supported by the underlying superconductor.

The second layer in this process is the metal bonding pads. In general, electroplated gold films provide a better surface than evaporated films for wire bonding. Most of this advantage is due to the fact electroplated films can be deposited much thicker than evaporated films. Electroplated films can be several microns thick, while it is difficult to evaporate more than one micron. Several attempts were made to deposit an electroplated gold surface onto the top of the bonding pads using a technique that was developed for electroplating gold pads onto a glass surface. However, the YBCO adhesion to the substrate was too delicate for this process which involved a short ultrasonic burst in acetone. In the end, the pads for the working devices were made by a bi-layer lift-off evaporation process. The details for this process are explained by Wentworth [13]. A 150 Å layer of chromium was first evaporated in order to enhance adhesion to the YBCO. Next, a 6000 Å layer of silver was evaporated, followed by a

2500 Å layer of gold. All evaporated films were deposited at a rate of 10 - 20 Å per second. The vacuum system used was a three hearth e-beam evaporator, which allows three metals to be evaporated in succession without opening the system to air. The system was pumped down to a base pressure of $\sim 1 \times 10^{-7}$ torr before evaporation began.

The third layer is an 800 Å dielectric film of sputtered SiO₂. This layer was patterned by sputtering through a stainless steel shadow mask that was clipped to the surface of the chip. The shadow mask confined the SiO₂ to a thin strip across the center of the chip (over the YBCO detector lines), while shielding the rest of the chip. An etching solution was used to etch the slot through the stainless steel for this process. An ordinary office staple was used to define the slot on the shadow mask by placing the staple on the resist covered blank stainless steel chip during UV exposure, and developing the image using an image reversal technique.

The sputtering was done using the same vacuum system that was used during the evaporation step. A Sputtered Films Research S-Gun was used for this process using an RF power source. The films were deposited at a power of 450 watts at a rate of ~ 0.4 Å/sec. The gas pressure during sputtering was probably near 5 millitorr, but this value was measured by a baratron pressure gauge which was not accurate in this pressure range. The best dielectric films were obtained by venting an argon/air mixture into the chamber during deposition with flow rates of 12 sccm and 0.3 sccm respectively.

For the final layer, the antenna leads and the heater were fabricated using a single evaporation lift-off step. Figure 4.10 illustrates how a photoresist air-bridge technique was used to define both the antenna and heater regions using a single lithographic step.

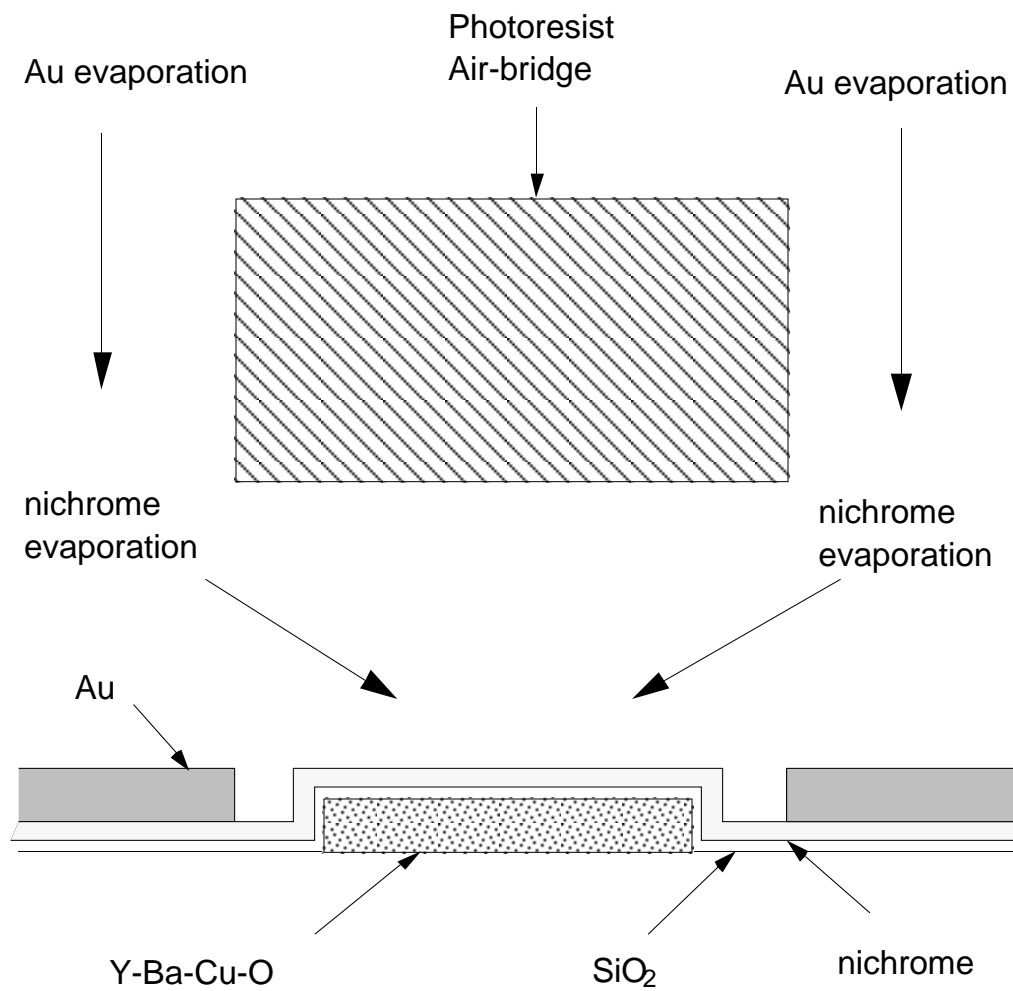


Figure 4.10 Photoresist air-bridge technique used to define the nichrome heater and antenna leads.

In this process, the same bi-layer lithographic process was used that was used to pattern the evaporated contact pads. The lower resist layer was developed such that it undercut completely over the detector region. This left a gap between the YBCO detector and the upper photoresist layer. By tilting the substrate, the heater material (nichrome) could be evaporated into this gap and onto the detector. The gold antenna leads were evaporated while the substrate was held flat, and thus the detector was shielded from the gold by the photoresist air-bridge. This layer required a careful alignment of the air-bridge over the detector. Figure 4.11 shows an optical micrograph of the final device. The gold antenna leads are visible as the two funnel-shaped bright regions pointing toward the center of the picture. The nichrome is the gray material that surrounds the antennae and connects them in the center. The YBCO film is shown as the two dark funnel shapes that are perpendicular to the antenna leads. The YBCO detector element is underneath the heater element. The antenna leads are approximately $2.5\ \mu\text{m}$ across near the tips. The heater and detector are separated by a $800\ \text{\AA}$ transparent layer of sputtered SiO_2 .

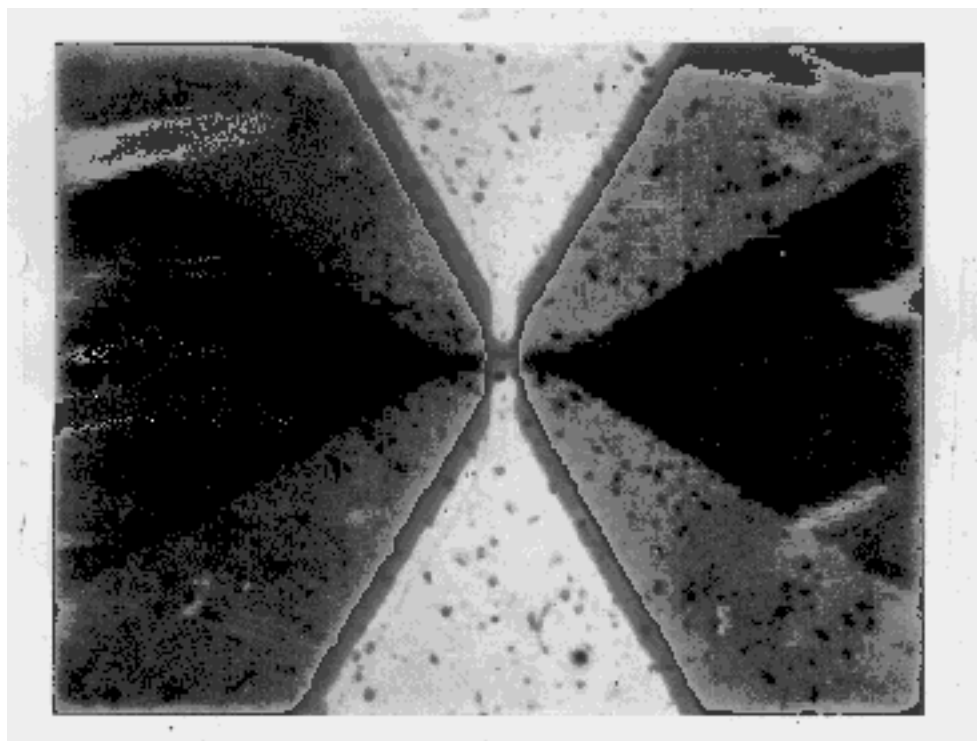


Figure 4.11 Optical photo of a YBCO composite microbolometer.

4.6 Cryogenic Apparatus

Once the devices were fabricated, the chip was then mounted inside a cryogenic probe for electrical testing. Silver paint was used to physically and thermally secure the chip to a copper block that acted as a nearly isothermal mass for the probe head. A silicon diode thermometer and a $25\Omega/25$ watt heater were mounted onto the probe to monitor and control the temperature of the copper block. The probe heater on the copper block is not to be confused with the small antenna heater on the microbolometer. The probe head was made removable by mounting electrical disconnects on the bottom side of the copper block. The disconnects were made from modified wire-wrapping sockets that were connected to grouped wire-wrapping posts that were soldered to wires leading to outside of the system. No actual wire wrapping was involved; the sockets (purchased from Radio Shack) provided compact and reliable electrical connections down to liquid nitrogen temperatures. Colder temperatures were not tested. The removable probe head allowed the chip to be bonded to the probe while mounted in the probe head. An ultrasonic ball bonder was used to bond gold wires to pads on the chip. The other end of the wires were either wedge bonded or silver painted to a pc board that was mounted on the probe head.

Once the sample was bonded to the probe head, the head was attached to a narrow stainless steel tube. The tube was used to suspend the probe head near the bottom of a long, narrow, air-tight canister. The probe head was cooled by lowering the base of this canister into liquid nitrogen. The canister was evacuated by a rotary vacuum pump and purged with helium gas before cooling to avoid water condensation on the inside of the canister. The canister was then backfilled to ~ 1 torr of helium to allow thermal conduction between the probe head and the walls of the canister. Wires from the probe disconnects led up the center tube to a 20 conductor feedthrough at the top of the system. A diagram of this system is illustrated in figure 4.12.

The temperature of the probe head could be controlled by either changing the pressure of the helium inside the canister, or by dissipating power in the heater on the probe head. A Lakeshore Cryotronics temperature controller (model DRC81C) was used to monitor and control the temperature of the probe head with the silicon diode temperature sensor (DT-470-BO-13) attached to the copper block.

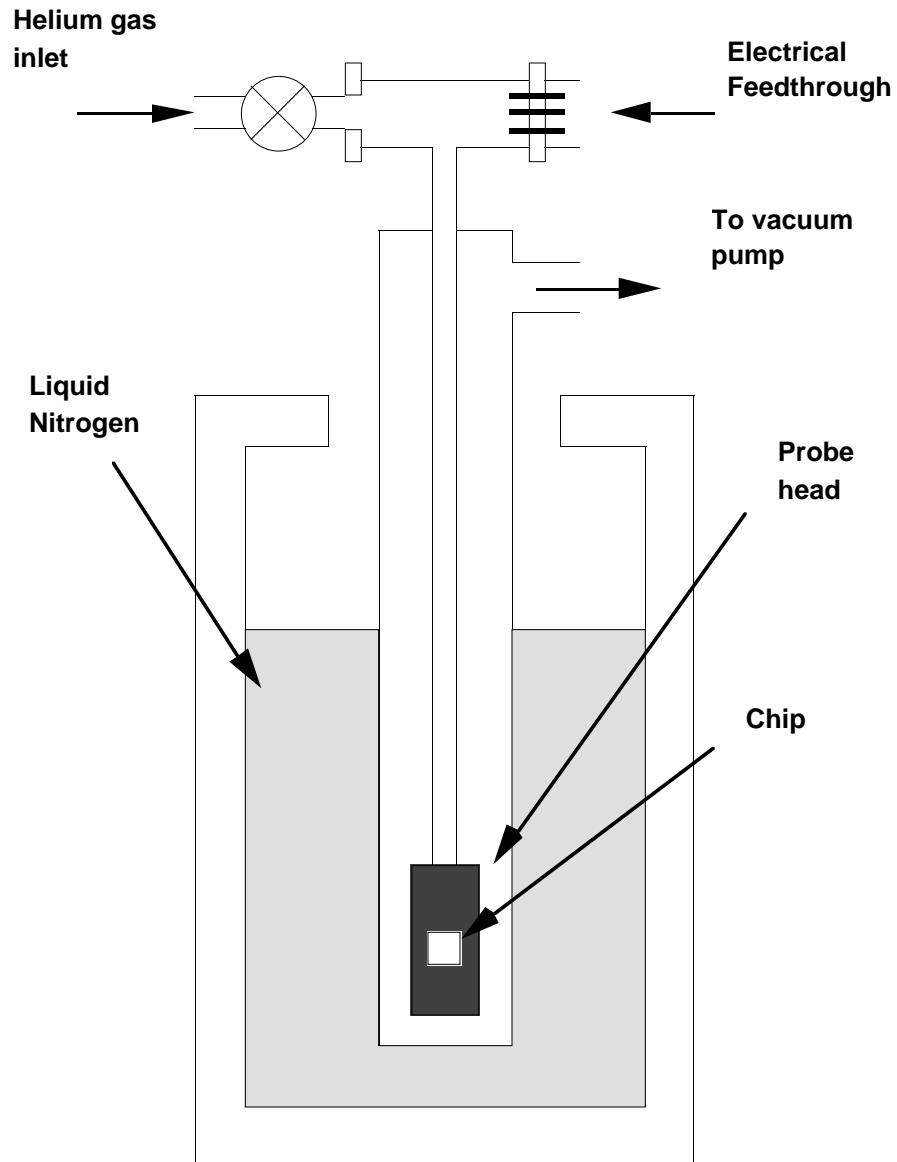


Figure 4.12 Apparatus for making microbolometer measurements at cryogenic temperatures.

4.7 Resistance vs. Temperature Measurements

The first significant electrical characterization of the devices involved measuring the resistance versus temperature (R vs. T) for the YBCO detector line. This was done to verify that the YBCO film survived the processing, and to measure the quality of the film. In a damaged film, the slope of the resistivity in the transition region may be reduced, and the temperature at which the resistance equals zero may be reduced or non-existent.

Most of the R vs. T measurements used a Stanford Research SR570 lock-in amplifier to measure the resistance during the measurement. Each detector line had two separate bonding pads on each side of the line so that four point measurements could be made. When the lock-in amplifier was used, a 1 volt sine wave at 10 Hz was used to drive current through the detector. A 222.0 K Ω resistor was placed in series with the detector line ($< 200 \Omega$) so that the oscillator was essentially an AC current source of 4.5×10^{-6} A. This provided the detector line with a current density of ~ 600 A/cm². The voltage across the detector was measured by the lock-in amplifier through another pair of leads. A computer (via GPIB port) was used to simultaneously read the temperature of the probe from the Lakeshore temperature controller while reading the detector voltage from the lock-in amplifier. Figure 4.13 shows data from an R vs. T overlaid with a dR/dT for a detector line near the transition temperature.

Figure 4.13 reveals a T_c (R=0) at 85K, which matches the typical values of T_c reported by Alan Berezine for YBCO films grown on buffered sapphire substrates [16]. This suggests that the films survive the processing steps very well. Figure 4.14 shows the R vs. T plots for various current densities. The currents in figure 4.14 correspond to currents that would be used during normal detector operation. It is important to note that the temperatures shown here correspond to the ambient temperature of the probe sensor, and not necessarily the temperature of the detector film. The apparent decrease in transition temperature at higher currents may be due to either non-thermal effects of the increased current density, or from joule heating of the detector line. Most importantly, this plot shows that the detector line remains sensitive to small changes in temperature even at higher currents.

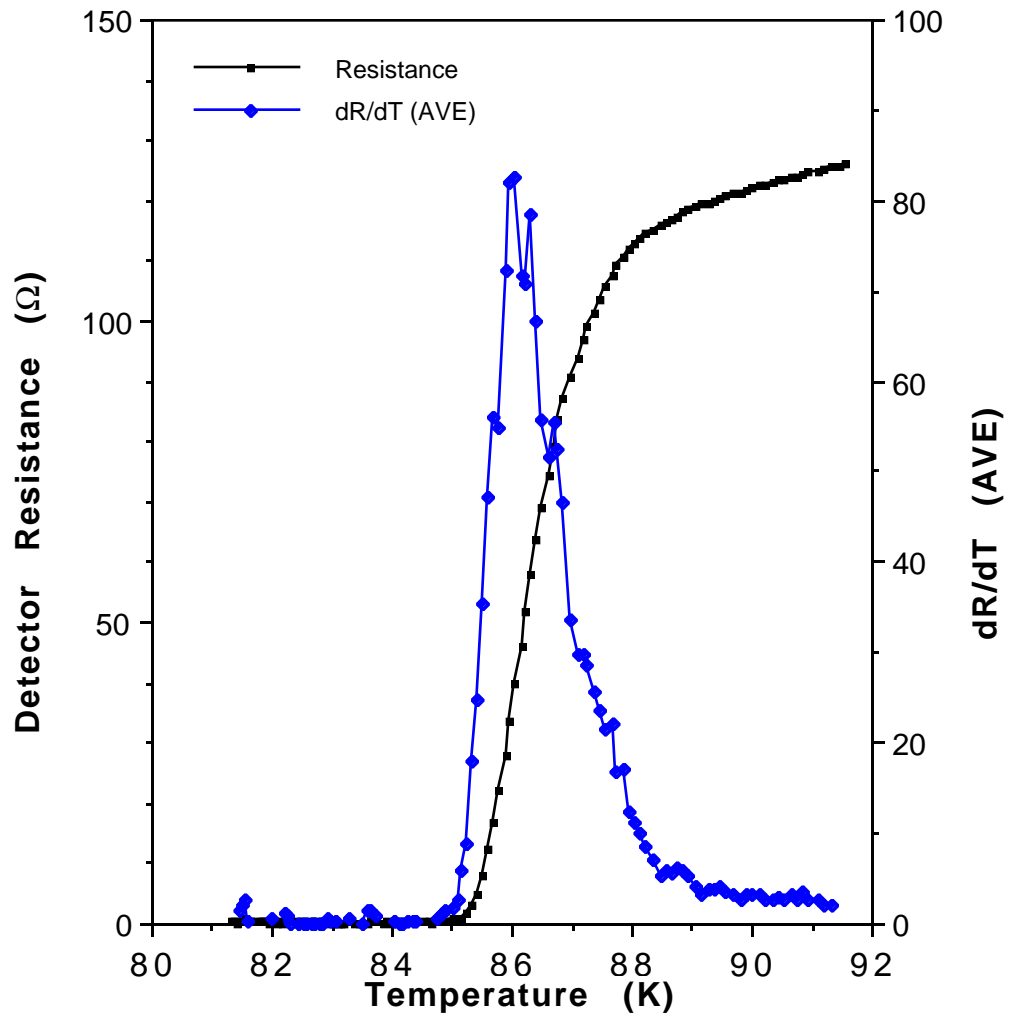


Figure 4.13 Resistance versus Temperature measurement overlaid with dR/dT for a YBCO detector line near the transition temperature. A current density of 600 A/cm^2 was used for a total current of $4.5 \times 10^{-6} \text{ A}$

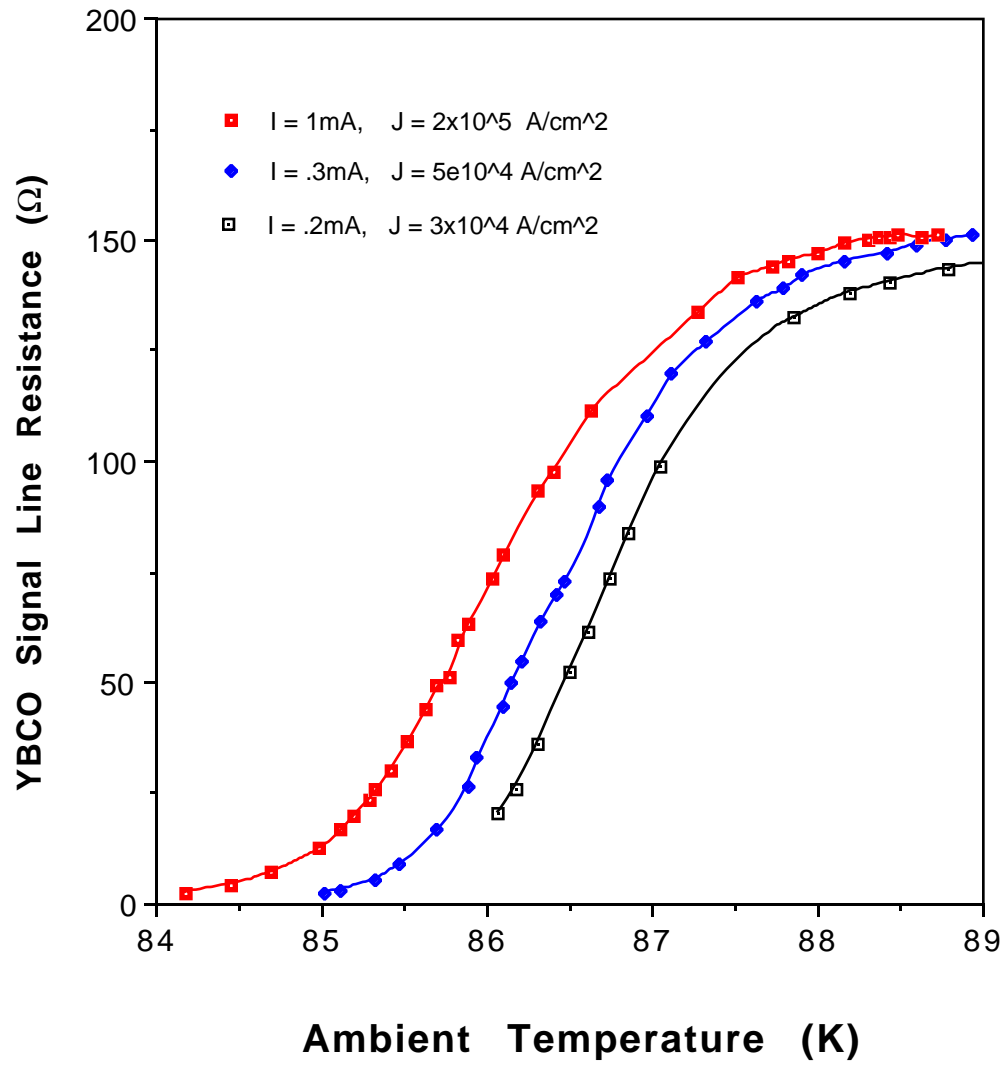


Figure 4.14 Resistance versus temperature of the detector line at various current densities.

4.8 Responsivity Measurements

To measure the electrical responsivity of the composite microbolometers, incident power in the heater was simulated by a DC current. The detector bias was held constant and its voltage was measured as power was ramped through the heater. Using this technique, the responsivity could be measured by measuring the slope (volts/watt) of a plot of detector voltage versus heater power.

A schematic of the apparatus used to make responsivity measurements is shown in figure 4.15. A four point measurement was performed simultaneously for both the heater and detector elements, requiring a total of eight terminals for each device. A schematic for this measurement circuit is given in figure 4.16. Circuits inside the probe are contained with the dashed line. The detector was biased with a constant low-noise current by using a battery powered current source. This current source was actually a 6 volt battery with a variable resistor circuit ($\sim 6 \text{ KW}$) in series. The detector voltage was read by a Keithley 195A digital multimeter connected to the detector through a separate pair of bonding pads.

The heater bias power was controlled by an HP 4140B. The voltage source from this instrument was used to drive the power while the current meter read the current through the heater. In order to obtain very fine increments in voltage across the heater element, a 1.2 KW resistor was placed in series with the heater element. The actual voltage across the heater was read by a Keithley 617 electrometer. One lead from each the detector and one lead from the heater were grounded to reduce the chance of accidentally stressing the dielectric between the two elements. A computer was used to control the instrumentation and to store data for these measurements.

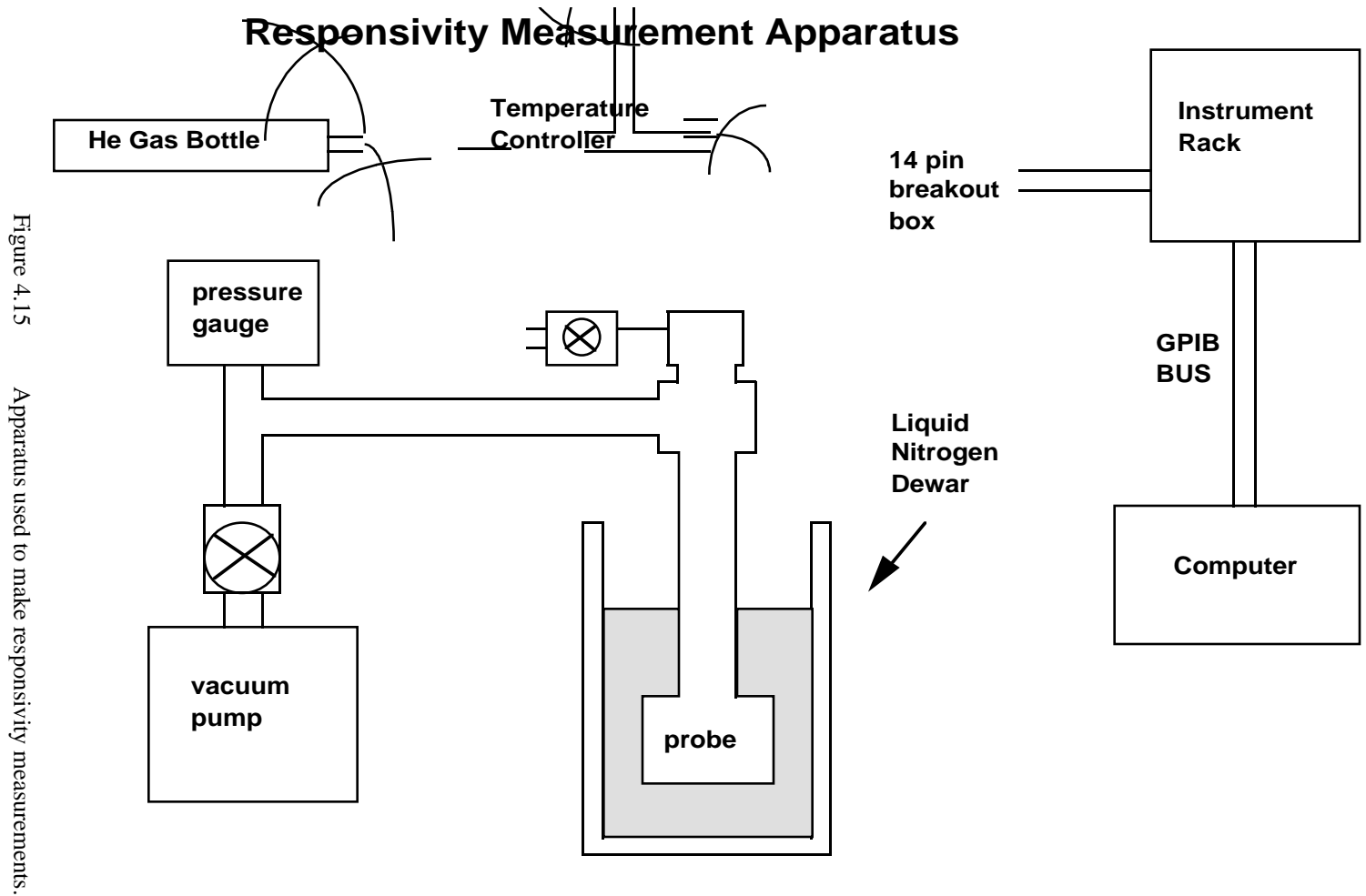


Figure 4.15

Apparatus used to make responsivity measurements.

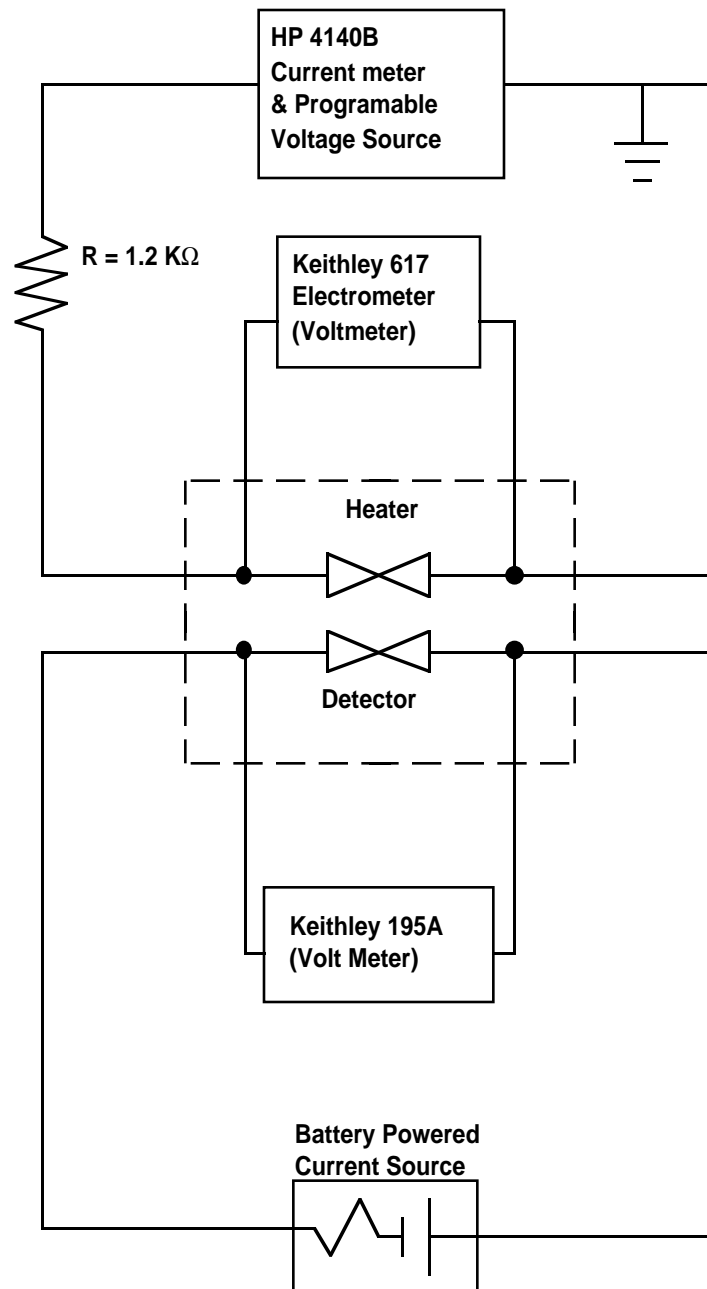
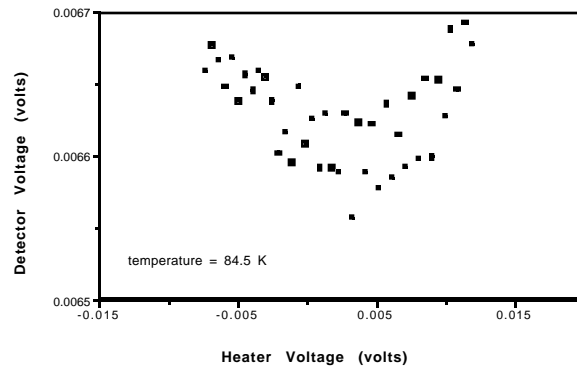


Figure 4.16 Schematic of the circuit and instrumentation used to make responsivity measurements.

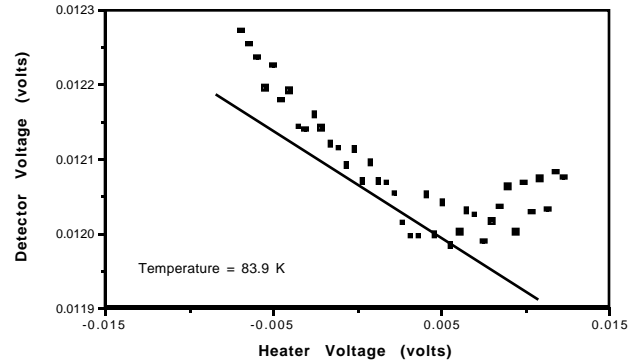
To obtain direct responsivity measurements of superconducting microbolometers, it is important to maintain nearly constant temperature during the measurement. Unfortunately, the Lakeshore controller broke down before these measurements were made. The probe temperature could be read, but the box could not be used as a temperature controller with the 25 watt probe heater. The probe heater was therefore controlled with a manual power supply to partially overcome this problem. Temperature drifts, sometimes as high as ~ 0.14 K, during the 5 - 10 second measurement time, were sometimes larger than the temperature changes induced by the microbolometer heater signal during measurement. Therefore, responsivity measurements required subtracting the thermal drift component from the data

One assumption made was that the rate of temperature change during the measurement (and between each data point) remained constant throughout the measurement. The time constant for the probe head was on the order of minutes, therefore this assumption should be accurate. It was also assumed that the resistance change due to probe temperature drift varied linearly with temperature drift. The data in figure 4.14 shows that the change in slope over a 0.15 K temperature range remained reasonably small throughout the transition. Therefore, the detector response due to heater signal can be extracted as a deviation from a linear change in resistance over time.

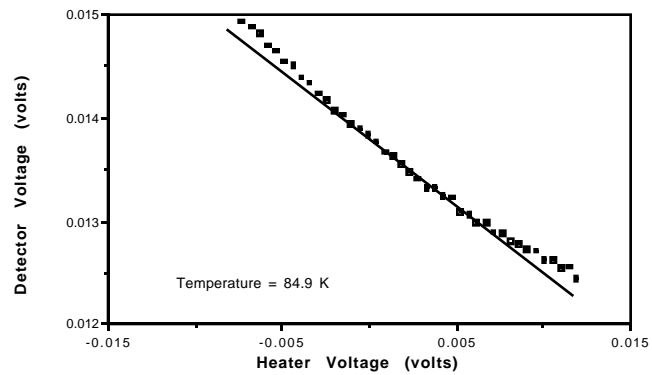
Figure 4.17 shows the detector voltage versus heater voltage for various degrees of temperature drift during the measurement. The responsivity extraction assumed that the heater current varied linearly with time. The detector voltage signal due to the heater signal is represented as the deviation from the lines shown in figures 4.17 b and c.



a) Negligible temperature drift



b) Noticeable temperature drift



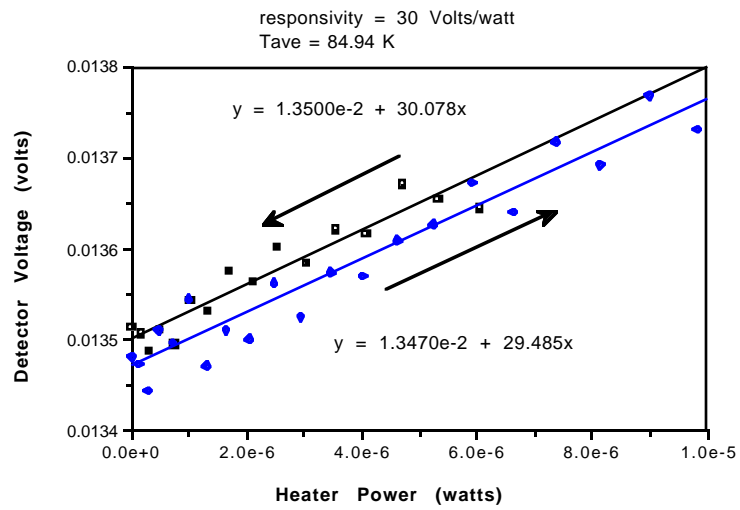
c) Significant temperature drift

Figure 4.17 Detector Voltage (V_D) versus Heater Voltage (V_H) data for various degrees of temperature drift during the measurement.

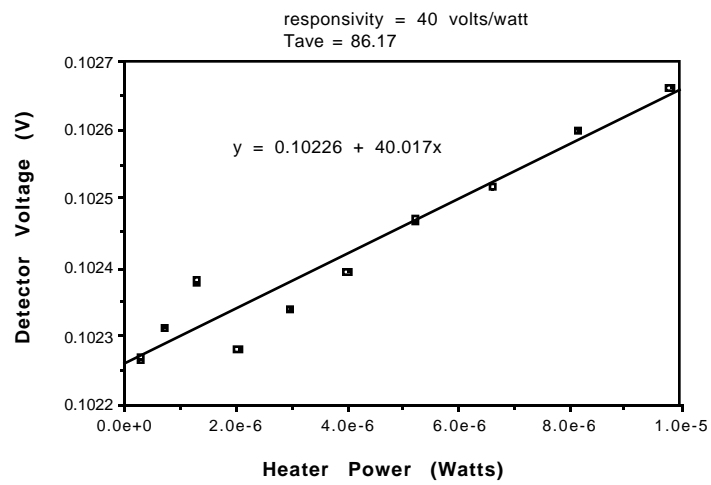
In all the responsivity measurements, the heater was biased with both negative and positive bias. For bolometers with a positive temperature coefficient of resistivity (as is the case for superconducting bolometers), the temperature increase due to incident power will cause an increase in detector resistance. For small signals, power will cause a linear increase in resistance, with a minimum at zero power. Using these assumptions, the effective detector voltage can be given as

$$V_d^{\text{eff}} = V_d^0 - \left(\frac{dV_d}{dV_h} \right) \cdot V_h \quad (4.2)$$

where V_d^0 is the detector voltage at zero incident power. Figure 4.18 a shows a plot of V_d^{eff} versus heater power (P_h) that was used to extract a responsivity value from the data shown in figure 4.17 c. The value of $\left(\frac{dV_d}{dV_h} \right)$ was adjusted until the slopes of the negative and positive bias curves were nearly equal. The responsivity was measured as the slope of the two lines. Figure 4.18b shows a less cluttered V_d^{eff} versus V_h plot, with only one leg of the power ramp shown.



A) Negative to positive heater bias



B) Zero to positive heater bias

Figure 4.18 Effective Detector Voltage (V_d^{eff}) versus Heater Power (P_h)

Figure 4.19 shows a plot of responsivity versus temperature overlaid with a plot of dR/dT . This plot shows that these results generally agree with expectations that the responsivity would be at a maximum where dR/dT is at a maximum. These values of responsivity are about a factor of four better than predicted by the numerical simulations for a highly conductive substrate (see figure 4.8). The data here shows a maximum responsivity of 40 V/W, while the numerical simulations predicted ~ 10 V/W for a substrate of $k = \sim 10$ W/cm/K. If these measured responsivity values are accurate, then this increase in responsivity may be explained by the existence of a thermal barrier at the YBCO/substrate interface [7-9]. Even if these maximum values are accurate, this is still only a marginal improvement over conventional bismuth microbolometers.

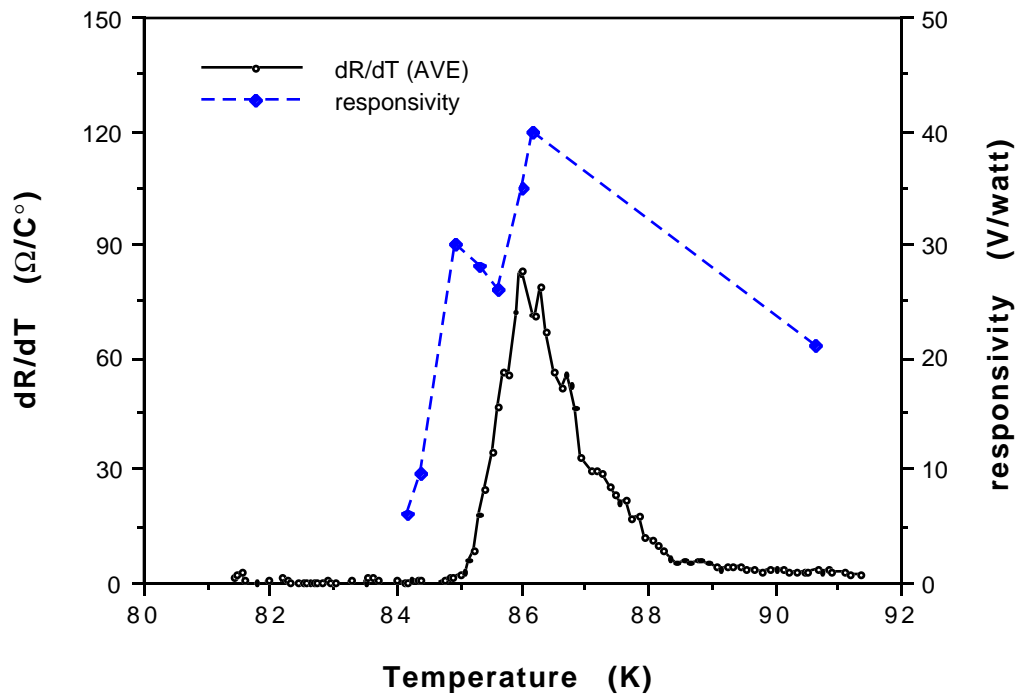


Figure 4.19 Responsivity as a function of temperature overlaid with a plot of dR/dT .

4.9 Noise Measurements

Noise measurements were made with a Stanford Research SR 570 lock-in amplifier while the detector was biased at 1 mA. The lock-in measured the noise across the detector voltage terminals over a 10% bandwidth of the selected frequency. Figure 4.20 shows the voltage noise $(V_n/\sqrt{\text{Hz}})$ as a function of frequency for a few temperatures in the transition region. The decreasing noise with frequency suggests that $1/f$ noise is dominant for this device. The solid line shows the slope for a perfect $1/f$ dependence. The bump in the data at 100 Hz may be due to 60 Hz noise within the room. Since $1/f$ noise is often caused by interfaces, the noise in these devices might be improved by annealing the bonding pads onto the YBCO surface, instead of using the thin chrome layer that was evaporated to promote adhesion. $1/f$ noise has also been reported to be the primary performance limitation for large area high T_c superconducting bolometers, even when contact pads were annealed to the superconductor [18].

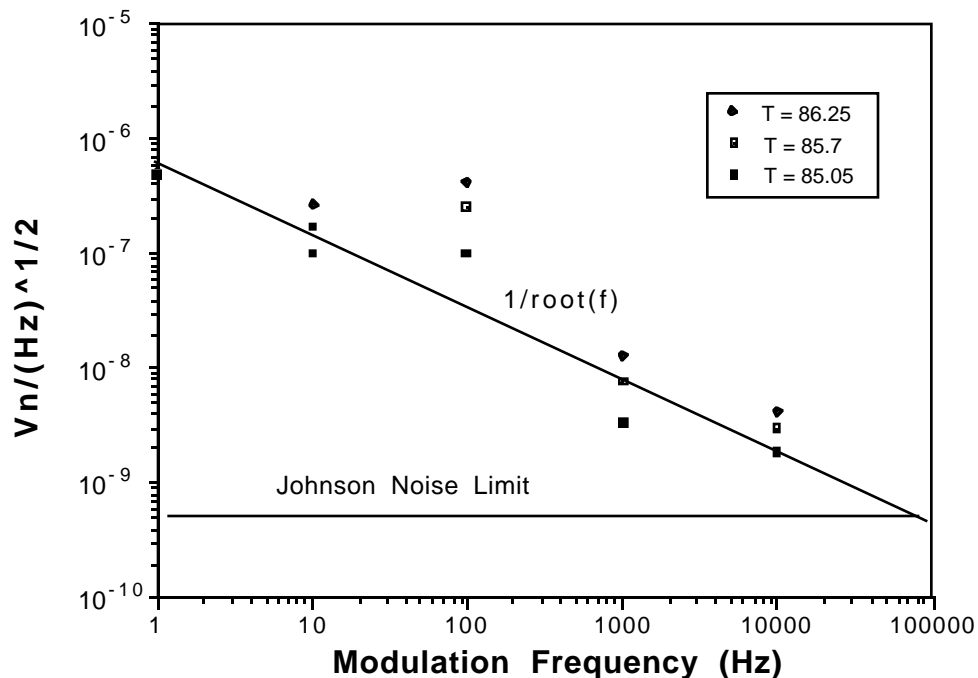


Figure 4.20 Voltage noise as a function of frequency for a YBCO detector line. The noise was measured over a bandwidth of 10% of the selected frequency.

If the responsivity is known as a function of frequency, the noise equivalent power (NEP) can be calculated by dividing the voltage noise by the responsivity.

$$\text{NEP} \left[\text{W} / \sqrt{\text{Hz}} \right] = \frac{V_n / \sqrt{\text{Hz}}}{r} \quad (4.3)$$

The actual frequency dependent responsivity was not measured for these devices, but was estimated by using the normalized numerical data shown in figure 4.9, using a dc responsivity of 40 volts/watt. Figure 4.21 shows a plot of NEP versus frequency calculated by using the noise data from figure 4.20 and a normalized dc responsivity. At 10 kHz, the NEP of $\sim 5 \times 10^{-11} \text{ W} \cdot (\text{Hz})^{-1/2}$ is comparable to what was reported for airbridge microbolometers ($2.8 \times 10^{-11} \text{ W} \cdot (\text{Hz})^{-1/2}$) [19] at 100 kHz, and $10^{-10} \text{ W} \cdot (\text{Hz})^{-1/2}$ for conventional bismuth microbolometers on glass. If the thermal response from the measured devices was enhanced due to a thermal barrier at the YBCO-substrate interface, then the detector speed may be slower than the numerical model shows, and thus the actual NEP could be lower than predicted by figure 4.21. However, since the simulated 3dB cut-off frequency of the composite structure on sapphire at 80 K was 10 MHz, a moderate thermal barrier would be unlikely to significantly affect the response at 10 kHz.

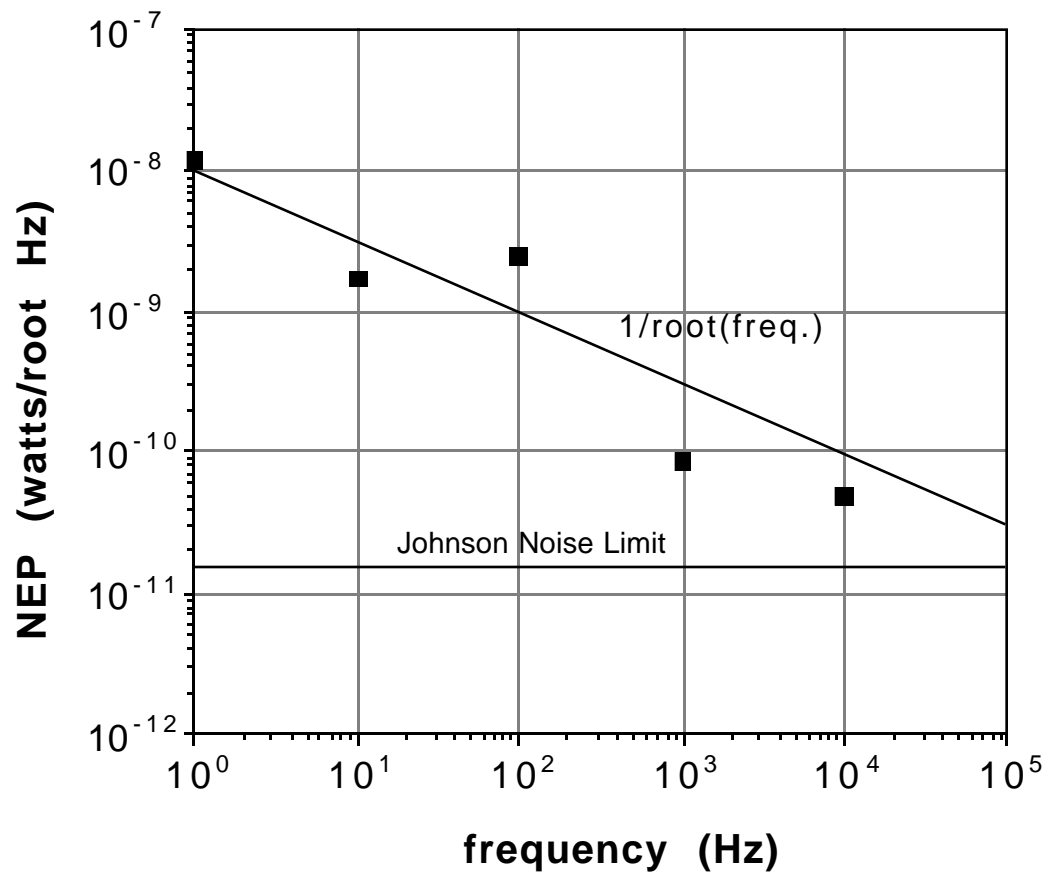


Figure 4.21 Noise equivalent power for the YBCO composite microbolometer, based on voltage noise measurements, dc responsivity measurements, and simulated transient thermal response.

4.10

Summary

A composite microbolometer on sapphire using a YBCO detector element has been demonstrated. The responsivity of this device was measured at 40 volts/watt, which is marginally better than for conventional bismuth microbolometers of the same size (~ 20 volts/watt). Transient thermal simulations using a new three dimensional finite difference algorithm predicted a 3 dB cut-off frequency of 10 MHz, which is much faster than the ~400 kHz reported for a bismuth air-bridge microbolometer, and ~ 200 kHz for a tellurium based composite microbolometer on a glass substrate. Noise equivalent power (NEP) values were calculated using voltage noise measurements, the dc responsivity measurement, and simulated transient thermal responses. This method predicted an NEP of $\sim 5 \times 10^{-11}$ at 10 kHz, which is comparable to what was reported for airbridge microbolometers ($2.8 \times 10^{-11} \text{ W}\cdot(\text{Hz})^{-1/2}$) at 100 kHz, and $10^{-10} \text{ W}\cdot(\text{Hz})^{-1/2}$ for conventional bismuth microbolometers on glass substrates.

The responsivity measurements demonstrated one of the difficulties in using transition edge detectors: that precise control of the ambient temperature is critical. One way of possibly dealing with this problem would be to use the antenna load to fine tune the detector temperature. By passing a dc current through the load, the load could be used to heat the detector. If the load resistance was also temperature dependent, then the load could also be used as a thermometer to monitor the detector temperature. However, such a setup would further complicate the detector.

Steady state thermal simulations predicted that the responsivity would increase by a factor of seven by varying the thermal conductivity of the substrate from 1 w/cm/K to 0.14 W/cm/K. For substrate thermal conductivities above ~ 0.5 W/cm/K, the dc responsivity was nearly independent of substrate thermal conductivity.

References

1. P. L. Richards, J. Clarke, R. Leoni, P. Lerch, and S. Verghese, "Feasibility of the High Tc Superconducting Bolometer," *Appl. Phys. Lett.*, vol. 54, pp. 283 - 285, (3), 16 January 1989.
2. M. G. Forrester, "Optical Response of Epitaxial Films of YBaCuO," *Appl. Phys. Lett.*, vol. 52, pp. (25), 20 June 1988 1988.
3. M. Leung, P. R. Broussard, J. H. Claasen, M. Osofsky, S. A. Wolf, and U. Strom, "Optical Detection in Thin Granular Films of Y-Ba-Cu-O at Temperatures between 4.2 and 100 K," *Appl. Phys. Lett.*, vol. 51, pp. (24), 14 December 1987.
4. J. M. Lewis, "Optical Detectors Based on Superconducting Bi-Sr-Ca-Cu-Oxide Thin Films", Undergraduate Thesis, Massachusetts Institute of Technology, 1989
5. J. Talvachio, M. G. Forrester, and A. I. Braginski, *Photodetection with High-Tc Superconducting Films*. New York: Plenum, 1989.
6. D. P. Neikirk, "Integrated Detector Arrays for High Resolution Far-Infrared Imaging", Doctoral Dissertation, Californai Institute of Technology, 1983
7. M. Nahum, S. Verghese, and P. L. Richards, "Thermal Boundary Resistance for YBaCuO Films," *Appl. Phys. Lett.*, vol. 16, pp. 2034 - 2036, 14 October 1991.
8. S. Zeuner, H. Lengfellner, J. Betz, K. F. Renk, and W. Prettl, "Heat Propagation in High Tc Films investigated by Optical Response Measurements," *Appl. Phys. Lett.*, vol. 61, pp. 973 - 975, 24 August 1992.

9. C. G. Levey, S. Etemad, and A. Inam, "Optically Detected Transient Thermal Resonse of High Tc Epitaxial Films," *Appl. Phys. Lett.*, vol. 60, pp. 126 - 128, (1), 6 January 1992.
10. J. Mees, M. Hahum, and P. L. Richards, "New Designs for Antenna-Coupled Superconducting Bolometers," *Appl. Phys. Lett.*, vol. 59, pp. 2329 - 2331, 28 October 1991.
11. E. N. Grossman, J. E. Sauvageau, and D. G. McDonald, "Lithographic Spiral Antennas at Short Wavelengths," *Appl. Phys. Lett.*, vol. 59, pp. 3225 - 3227, 16 December 1991.
12. M. Nahum, Q. Hu, and P. L. Richards, "Fabrication and Measurement of High Tc Superconducting Microbolometers," *IEEE Transactions on Magnetics*, vol. 27, pp. 3081 - 3084, March 1991.
13. S. M. Wentworth, "Far-Infrared Microbolometer Detectors", Doctoral Dissertation, University of Texas at Austin, 1990
14. J. Heston, J. M. Lewis, S. M. Wentworth, and D. P. Neikirk, "Twin Slot Antenna Structures Integrated with Microbolometers," *Microwave and Optical Technology Letters*, vol. 4, pp. 15, (15), 5 January 1991.
15. S. M. Wentworth, and D. P. Neikirk, "Composite Microbolometers with Tellurium Detector Elements," *IEEE Trans. Microwave Theory Tech.*, vol. 40, pp. 196-201, February 1992.
16. A. B. Berezin, "A Low Noise High Temperature Superconducting Quantum Interference Device", Doctoral, The University of Texas at Austin, 1993
17. D. P. Neikirk, and D. B. Rutledge, "Air-bridge Microbolometer for Far-infrared Detection," *Appl. Phys. Lett.*, vol. 44, pp. 153-155, 15 January 1984.

18. R. W. Zindler, and R. R. Parsons, "1/f Noise in BiSrCaCu-O and Its Impact on Bolometer Performance," *Journal of Vacuum Science Technology A*, vol. 10, pp. 3322-3324, Sep/Oct 1992.
19. D. P. Neikirk, W. W. Lam, and D. B. Rutledge, "Far-Infrared Microbolometer Detectors," *International Journal of Infrared and Millimeter Waves*, vol. 5, pp. 245 - 278, 3 1984.